Published in final edited form as:
Nanotechnology. 2014 November 7; 25(44): 445104. doi:10.1088/0957-4484/25/44/445104.

Highly stable polymer coated nano-clustered silver plates: A multimodal optical contrast agent for biomedical imaging

Aniruddha Ray[1,#], **Ananya Mukundan**[1], **Zhixing Xie**[2], **Leshern Karamchand**[1], **Xueding Wang**[2], and **Raoul Kopelman**[*,1]

[1]Department of Chemistry and BioPhysics, University of Michigan, Ann Arbor

[2]Department of Radiology, University of Michigan Medical School, Ann Arbor

Abstract

Here we present a new optical contrast agent, based on silver nanoplate clusters embedded inside a polymer nano matrix. Unlike nanosphere clusters, which have been well studied, nanoplate clusters have unique properties due to the different possible orientations of interaction between the individual plates, resulting in a significant broadening of the absorption spectra. These nanoclusters were immobilized inside a polymer cladding, so as to maintain their stability and optical properties under in vivo conditions. The polymer coated silver nanoplate clusters show a lower toxicity, compared to the uncoated nanoparticles. At high nanoparticle concentrations, cell death occurs mostly due to apoptosis. These nanoparticles were used for targeted fluorescence imaging in a rat glioma cell line by incorporating a fluorescent dye into the matrix, followed by conjugation of a tumor targeting F3 peptide. We further used these nanoparticles as photoacoustic contrast agents in vivo, to enhance the contrast of the vasculature structures in a rat ear model. We observed a contrast enhancement of over 90%, following nanoparticle injection. It is also shown that these NP's can serve as efficient contrast agents, with specific targeting abilities, for broadband multimodal imaging, usable for diagnostic applications and extendable into use as therapeutic agents as well.

Keywords

Polymer Nanoparticles; Silver Nanoplates; Metal Nanocluster; Fluorescence Imaging; Photoacoustic Imaging

INTRODUCTION

Noble Metal nano-clusters (NC's) have attracted great interest due to their unique optical properties, which arise due surface plasmon resonance (SPR)[1,2,3]. The phenomenon of SPR arises from oscillations of surface electrons when irradiated with an appropriate wavelength of light[4]. In addition to their unique optical properties, the point of contact between the metal nanoparticles is generally characterized by a high electric field, due to the near field coupling of surface plasmons, which has been exploited for enhancing fluorescence and

[*]Corresponding author, kopelman@umich.edu.
[#]Present address: National Institute of Standards and Technology, Boulder, Colorado.

Raman signals by several orders of magnitude[5,6,7,8]. Other applications of the noble metal NC's include photoacoustic imaging, photoluminescence, photochemistry of molecules, and improving the reaction kinetics[9,10,11].

Metal nano-clusters may involve ensembles of noble metal nanoparticles of various shapes and sizes, such as gold or silver spheres, rods and pyramids[12,3]. It is usually difficult to perform controlled aggregation so as to achieve the specifically desired optical properties; however an even greater challenge is maintaining the stability and optical properties of these aggregates under biological conditions. The latter is particularly difficult to achieve and has limited the translation of these NC's towards applications *in vivo* and in cells. The NC's tend to aggregate under *in vivo* conditions, or in the presence of ions and proteins, leading to reduced stability and to an instantaneous change in their optical properties. In addition to the issue of stability, other drawbacks include induced cytotoxicity and an inability to achieve selectivity towards any specific cell line of interest.

Here we present a method for stabilizing clusters of silver nanoplates, towards *in vivo* applications, by encapsulating them in a polyacrylamide matrix. Recently, clusters of gold nanospheres, embedded in silica or polystyrene nanoparticles, were utilized for dual mode tumor imaging, and for plasmonic applications, respectively[13,14]. We chose silver nanoplates as they have recently gained considerable attention as optical contrast agents, due to their unique optical properties that can be tuned by controlling the aspect ratio of the particles[15].They have been used for photoacoustic imaging, plasmon resonance chemical sensing, as well as for enhancing fluorescence and Raman signals[16,17,18,19]. However, most of these utilities have been limited to *in vitro* applications. Only a few reports exist on the application of silver nanoplates for *in vivo* applications. Embedding the NC's inside a polymer matrix provides excellent stability and preserves their optical properties, facilitating their use *in vivo*, e.g. for test animals. Some of the advantages that the polyacrylamide matrix confers to the nanoclusters and its contents are:

1. Protecting the metal surface and thus preventing changes in optical properties caused by adsorbed molecules or proteins, which might modify the SPR properties of the metal *in vivo*.
2. Maintaining the structural stability of these NC's under biological conditions.
3. Enabling delivery of multiple agents to the same location without the need to modify the metal's surface.
4. Enabling specific targeting towards any particular cell line of interest.
5. Having the ability to prevent the NC's from acting as catalytic agents in the body, by preventing them from interacting with proteins and molecules; this potentially reduces their toxicity.

In addition to the above advantages, coating silver nanoplates with silica, an inorganic polymer, has been shown to prevent chemical etching by chloride ions abundantly present in biological systems[20]. Recently it was also demonstrated that polymer coating of gold nanoplates improves their photothermal stability when exposed to a pulsed or continuous wave laser; this is an extremely desirable property for optical contrast agents[21].

The composite NP's presented here were prepared by first stabilizing the NC's in aqueous phase droplets containing monomers, followed by polymerization of the monomer. These NP's show good optical stability over time, as monitored over a week. In addition to nanoplate clusters, this method can also be used to incorporate silver nanosphere clusters or even single silver nanoplates into the PAA matrix. We also present a detailed toxicity study involving the effects of these NP's on the 9L cancer cell line; the study includes looking into cell death mechanisms and comparing the toxicity of these NP's with that of uncoated silver nanoplates. These polymer coated NP's were further conjugated with tumor targeting F3 peptides, so as to specifically target the NC's to tumor cells. The feasibility of using these NP's for targeted fluorescence imaging was demonstrated by adding a fluorescent dye, Rhodamine 6G, into the matrix and imaging a rat glioma cell line. The presence of the metal core helps retain the fluorescent dye inside the matrix. These NP's were further utilized for *in vivo* photoacoustic microscopy as a method of improving optical contrast. We observe better than 90% enhancement in optical contrast from blood vessels in a rat ear. Our results show that this contrast agent can also be easily tailored for *in vivo* optical imaging applications, and thus opens the possibility of exploiting various optical enhancement mechanisms *in vivo*. In addition, these NP scan be used for X-Ray/CT imaging, as well as for therapeutic applications, such as photothermal therapy.

MATERIALS AND METHODS

Materials

Acrylamide, methylene-bis-acrylamide (MBA), dioctylsulfouccinate (AOT), Brij 30, hexane, ammonium persulfate (APS), N,N,N',N'-tetramethylethylenediamine (TEMED), bovine serum albumin (BSA) (30% w/v) and L-cysteine were all acquired from Sigma-Aldrich (St. Louis, MO). 3-(aminopropyl)methacrylamide hydrochloride salt (APMA) was obtained from Polysciences Inc. (Warrington, PA). Ethanol (95%) was acquired from Decon labs, Inc (King of Prussia, PA). The silver nanoplates were obtained from Nanocomposix Inc. (San Diego, CA). All solutions were prepared in 18-MΩ water purified in a Barnstead 1 ThermolyneNanopure II system. All the chemicals and materials were used as received.

Preparation of the nanoparticles

The nanoparticles were prepared using a micro-emulsion and radical polymerization technique[22, 23]. This involves creation of aqueous phase droplets, containing monomers crosslinker and silver cluster, stabilized by surfactants in an oily (Hexane) solution. The aqueous phase contained monomers—acrylamide(8.6 mmol), APMA (0.25mmol), MBA(1.2 mmol)and silver nanoplate cluster. The clustering of the silver nanoplates can be induced in different ways such as exposure to light, repeated freeze thaw cycle or chemically. In this case the clustering of the plates was induced by adding MBA to the nanoplates followed by sonication at 40°C. This solution was then added to a 36 ml hexane solution containing 6.85 mmol Brij-30 and 2.88 mm dioctyl-sulfosuccinate. The two solutions were emulsified by stirring them for 20 min under an inert (Ar) atmosphere. The reaction was initiated by using 0.54 mmol TEMED and 28 μmol APS, freshly prepared 10% (Weight/Volume) in water. The solution was further stirred for two hours, under an inert atmosphere so as to complete the polymerization. Hexane was removed by rotary evaporation, using a Rotavapor-R

(Brinkmann Instruments), and then suspended in ethanol. The surfactants and excess dye were removed by washing the particles six times in ethanol and water, respectively, in an Amicon ultra-filtration cell (Millipore Corp., Bedford, MA), using a 300 kDa filter, and then freeze-dried with a 5L ModulyoD freeze dryer (ThermoFisher Scientific).

The Rhodamine containing nanoparticles were prepared by post-loading the Rhodamine-6G dye into blank polyacrylamide nanoparticles, containing the silver core as described before[24]. The nanoparticles are then washed thoroughly in water a few times, to get rid of any extra dye, and then freeze dried.

The F3 peptide conjugation was performed by first attaching heterobifunctional PEG crosslinkers (2 kDa) to the NP's surfaces and then coupling the F3 peptides to the terminal ends of the PEG crosslinkers, using a published protocol[25].

Particle size

The particles were diluted in water at a concentration of 1 mg/ml, and the particle size distribution in aqueous solution was measured by dynamic light scattering (DLS), using a Beckman-Coulter Delsa Nano C submicron size analyzer.

ICP spectroscopy

The amount of silver encapsulated was determined by Inductively Coupled Plasma (ICP)-Optical Emission Spectroscopy, using a Perkin-Elmer Optima 2000 DV machine. The nanoparticle sample concentration was 2 mg/ml in water.

TEM

Transmission Electron Microscopy (TEM) was performed by using 0.01 mg/ml nanoparticle solutions and the negative staining of the polyacrylamide was done with Uranyl Acetate. The TEM was performed using a Philips CM-100 TEM microscope.

Fluorescence microscopy

The fluorescence images of the cells loaded with nanoparticles were taken using the Leica confocal microscope (SP-5X), located at the Microscopy image analysis Lab of the University of Michigan. The images were acquired using a 40X or 60X oil immersion objective in the confocal mode. Photo multiplier tubes (PMT) were used to collect the fluorescence in both cases.

Cell Culture Procedure

All cell viability assays were implemented with 9L cells, a rat brain gliosarcoma cell line, in vitro. The cells were kept in an incubator at 37°C with 5% CO2. The cells were cultured using Roswell Park Memorial Institute 1640 media (RPMI 1640-11875), augmented with 10% fetal bovine serum (FBS) and 1% antibiotic-antimycotic (anti-anti). The RPMI 1640 media, FBS, and the anti-anti were all purchased from Gibco®,Life Technologies.

MTT assay

The 9L cells were plated in a 96-well plate, with each well containing 2500 cells in 200 μL of RPMI media. The cells were incubated with the nanoparticles for 24 or 48 hours.

After the incubation period, the media was removed and replaced with 120 μL of fresh RPMI media, containing tetrazolium salt. Each of the wells received 100 μg of the tetrazolium salt [3-(4,5-Dimethylthiazol-2-yl)-2,5-Diphenyltetrazolium Bromide] (MTT). The cells were incubated for four hours, during which the MTT was reduced by the mitochondrial dehydrogenases, present in the live cells, into a formazan product with a maximum optical absorption at 550 nm. After four hours of incubation, the colorless RPMI media was removed and 100 μL of dimethyl sulfoxide (DMSO) was added to the wells, for solubilizing the formazan product. The absorption of the resulting solution was measured at 550 nm, with a Microplate Reader (Anthos 2010, Biochrom). The cell viability was calculated by comparing the relative absorption of the nanoparticle-incubated cells with control cells into which no nanoparticles were added.

Monitoring Oxidative Stress

To measure the oxidative stress in cells, the molecule dichlorodihydrofluoresceindiacetate (DCFH-DA) was used. DCFH-DA is oxidized into the fluorescent dichlorofluoresceinediacetate (DCF-DA), in the presence of reactive oxygen species, which allows for a quantitative measurement of ROS.

Cells were plated in 3.5 cm diameter glass bottom microwell dishes (2mL of cell suspension solution per dish) and incubated with the NP's (0mg/mL, 2mg/mL, 4mg/mL) for 24 hours. Following the NP incubation, the cells were incubated with DCF-DA solution (9.2μM) for 30 min, before then in fresh media. The dye solution was prepared by first dissolving the dye in ethanol and then in RPMI media. The fluorescence response of the DCF-DA in cells was monitored using a confocal microscope with an excitation wavelength of 496 nm and an emission wavelength range of 510-550nm.

Apoptosis and Necrosis

An AnnexinV-FITC/PI Assay was used to assess the mechanism of cell death. Cells were plated in an 8 well chamber with 300 μL of cell suspension (10,000 cells per well) in RPMI 1640 media. The cells were incubated with the NP (4mg/mL) for 24 or 48 hours. Following the NP incubation, the NP containing media was removed and replaced with media solution containing AnnexinV-FITC and PI. The solution was prepared with a concentration of 15 μM of PI and with 120 μL of FITC conjugated AnnexinV, solubilized in 800μL of Dulbecco's Modified Eagle Medium (DMEM). The media was supplemented with 10% FBS and 1% anti-anti.

The fluorescence response of the AnnexinV-FITC was monitored using a confocal microscope with an excitation wavelength of 488 nm and an emission wavelength range of 500-550 nm. The fluorescence response of the PI was measured with an excitation wavelength of 535 nm and an emission wavelength range of 615-630 nm.

Photoacoustic imaging *in vivo*

The *in vivo* imaging of the vasculature in the ear of Sprague-Dawley rats was performed, using a photoacoustic microscope as described before[26, 27]. An Nd:YAG laser (Spot-10-200-532, Elforlight Ltd, UK) working at a 532 nm wavelength has a pulse duration of 2 ns and a repetition rate (PRR) of 1 KHz. The laser light was spatially filtered by an iris and then expanded into a parallel beam, which was rastered over the tissue object by 2D Galvanometers. The intensity and the stability of the laser beam was monitored and calibrated by a photodiode (DET10A, Thorlabs, NJ). An achromatic lens with a focal length of 50 mm was used as the objective lens. Photoacoustic signals were detected by a commercial calibrated needle hydrophone (HNC-1500, Onda, CA) with a10 dB bandwidth, of 300 kHz-20 MHz. The detected photoacoustic signals, amplified by a low noise amplifier (AH 2010, Onda, CA), were digitized by an A/D card (Razor CS14X2, GaGe, IL) for reconstructing the image. The spatial resolution of this system was measured by imaging an USAF resolution template (T-20-P-TM, Applied Image Inc, NY). Determined by the optical focusing, the lateral resolution was 5μm. Limited by the central frequency and bandwidth of the hydrophone, the axial resolution of this system was 105 μm. Before experiments, the hairs on the right ear of a Sprague Dawley rat (Charles River Labs, body weight: 200g) were gently removed, using a commercial human hair-removing lotion. During experiments, the animal was placed on a homemade animal holder, and a mixture of 1% isoflurane, with medical grade oxygen, was ventilated to the animal, through a commercial anesthesia system (SURGIVET ISOTEC 4, Smiths Medical, WI) at a flow rate of 1 l/min, to keep the animal motionless. The nanoparticle dose was varied between 100-120 mg/kg of rat weight. The nanoparticles were injected into the vein and the imaging performed 10 minutes after injection. The animal experiment has been approved by the UCUCA of the University of Michigan.

RESULTS and DISCUSSION

Preparation and characterization of the nanoparticles

The composite NP's were prepared using the technique of reverse micelle polymerization, as shown in Figure 1. Using this method we were able to encapsulate clusters of silver nanoplates, as shown in the TEM figure 2a. We observe that the nanoplates aggregate both laterally and axially. We used nanoplates that were mainly 30-50nm in size and the peak absorption wavelength is between 550 and 600 nm, as shown in figure S1. Following clustering, the peak wavelength shifted to 510nm and we also observe a significant broadening of the absorption spectra. The spectral width of the NP's is more than twice that of free nanoplates of similar dimensions. An absorption spectrum of the NP's is shown in Fig 2b. The spectral broadening at lower wavelengths (blue shift) is a result of the plates stacking up on top of each other, axially, effectively decreasing the aspect ratio. The broadening towards higher wavelengths (red shift) can be attributed to the lateral interaction of the nanoplates, which effectively increases the aspect ratio. This may account for the second peak observed at 740nm, in the absorption spectrum, with about 17% of the maximum's intensity. A comparison between the absorption spectra of the NP's, individual nanoplates and nanospheres, and the enhancement ratio in the visible region of the spectrum, is shown in Fig S1. Compared to the nanoplates the pure silver nanospheres have an

absorption maximum at 420 nm. The spectral properties can be tailored for a particular application by controlled aggregation[13]. In this study our aim was to demonstrate translation of such NC's towards applications to cells and animal models, so we have not attempted to perform controlled aggregation of the silver nanoparticles. Although challenging, such controlled aggregation has been achieved using methods such as viral scaffolds, polymer/protein as crosslinkers,etc[28,6,3].

The stability of the nanoparticles was tested, over a week, under biological conditions, as shown in Figure 2c. We observe only a 20% reduction in absorbance, in the optical spectrum. It has been previously shown that these types of PAA based nanoparticles accumulate inside the tumor within a few hours and can be retained for several days. Using this type of nanocluster contrast agent, which retains its optical properties for over a week, will enable continuous monitoring of biological activity over long periods of time.

Toxicity

Toxicity from silver nanoparticles is generally attributed to two mechanisms: Ag^+ ion shedding and/or toxicity solely attributed to the nanoparticles themselves[29]. In solutions, silver ions are continuously released from the nanoparticles and taken up by cells. These can interact with the proteins containing thiol groups in the mitochondria, which would inhibit respiratory function[30,31] and create oxidative stress, by generating reactive oxygen species (ROS). The increase of ROS has been reported to regulate cell death[32]. Similarly, silver nanoparticles have been shown to damage the structure of cell membranes and of the mitochondria, by mechanically disrupting membrane proteins and catalyzing oxidation-reduction reactions on such proteins[29,31]. In addition, silver ions and nanoparticles have both been shown to react with DNA and RNA, binding to sulfur and phosphorus-containing groups, causing cell death[30,33].

It has been shown that the shape of the nanoparticle impacts its biological properties[31, 34], and that silver nanoplates in particular are more toxic than nanoparticles with other shapes, such as nanospheres and nanowires[34]. The cytotoxicity from our NP's was evaluated using an MTT assay and is shown in Fig 3.

We do not observe any significant cytotoxicity from the NP's, up to a concentration of almost 2mg/mL, which is a significantly high local concentration. However, at higher concentrations, of 4mg/mL, considerable cytotoxicity was observed, for the 24 and 48-hour incubation periods. For both the uncoated silver nanoplate and NP cases, there was a slight increase in toxicity when going from the 24-hour incubation to the 48-hour incubation data. Overall, at lower NP concentration, slightly lower cytotoxicity was observed, in comparison to the uncoated silver nanoplates (Suppl. Section). The cytotoxicity of the nanoplates has been attributed primarily to their physical properties, particularly the crystalline structure of the nanoplates, in addition to Ag^+ ion shedding[31,34]. The crystalline structure of silver nanoplates, unlike that of nanospheres or nanowires, contains packing structures and defects that lead to a higher surface reactivity[31,34]. The higher electrocatalytic activity caused by these defects[34] can result in an increased tendency for the silver nanoparticles to bind to membrane and mitochondrial proteins, creating ROS, and thereby leading to cell death. The polyacrylamide coating has the potential to reduce this reactivity, by acting as a barrier

between the silver nanoplates and the cells, leading to a reduction in toxicity. This may be the reason for the somewhat lower cytotoxicity of the NP.

Next we monitored the onset of oxidative stress by looking at the dose dependence of the production of ROS in the cells, as shown in Fig 4. We observe a similar fluorescence signal for the 2mg/mL concentration and the control, indicating the absence of significant ROS production or oxidative stress. However, the fluorescence for the 4mg/ml concentration is more than twice that of the control, indicating a high level of ROS production and a significant oxidative stress in cells. Reactive oxygen species are produced when silver nanoplates and silver ions interact with mitochondrial enzymes that are involved in cellular respiration. Silver nanoplates and silver ions interact with the electron transport chain (ETC), during the oxidative phosphorylation stage of cellular respiration, facilitating the escape of electrons that are part of this chain, which then interact with oxygen to form ROS[30]. We observe an onset of oxidative stress after 24 hours, for the 4mg/ml concentration.

We also tested the cell death mechanism (apoptosis vs. necrosis) using the AnnexinV-FITC/PI assay. Apoptosis is programmed cell death, and does not lead to uncontrolled inflammation, while necrosis, i.e., cell death due to external factors, leads to an uncontrolled inflammatory response[34]. Uncontrolled inflammatory response generally causes additional problems; thus determining the cell death mechanism is vital for understanding the potential toxic effects of silver nanoplates *in vivo*. Figure 5 shows the percentage of cells undergoing apoptosis and necrosis, after 24 and 48 hours, when incubated with a 4 mg/ml NP concentration. We used the concentration of 4 mg/ml, since we observed cytotoxicity and oxidative stress at this concentration, based on the previous MTT assay and the ROS data. While both the 24 and 48-hour incubation samples contained a majority of apoptotic cells, the 24-hour sample contained 10% necrotic cells while the 48-hour sample contained 27% necrotic cells, almost three times the percentage of the 24-hour sample, as well as fewer apoptotic cells. This difference suggests that cells may initially undergo apoptosis and then turn necrotic, due to ongoing exposure to the NP. This may be because low levels of ROS trigger regulated cellular death while high levels can cause sudden disruption[32]. This increased accumulation time may damage the cell's ability to self-destruct in a controlled fashion, leading to necrosis rather than apoptosis. Thus cells that may initially start off as apoptotic may become necrotic after repeated ROS exposure[32]. However, we note that under *in vivo* conditions such cells are most likely to be taken up by macrophages, within 2-4 hours; well before they turn necrotic[35].

Fluorescence imaging

Targeted fluorescence imaging was performed on rat glioma cells by incorporating a fluorescent dye, Rhodamine 6G (Rh-6G), into the matrix. Rh-6G is highly soluble in both water and alcohol and thus has a tendency to leach out of the matrix during the NP washing steps. However, due to the presence of the silver NC's, the dye can be easily retained inside the matrix, making it feasible to perform fluorescence imaging in cells as well as *in vivo*. A fluorescence image of the 9L cells containing the nanoparticles is shown in Fig 6.

The presence of the metal cluster core can enhance the fluorescence of free dye molecules due to the presence of surface plasmon resonance. However, this involves a delicate balance that is dependent on the molecule's distance from the metal surface, as well as on the molecular orientation[36,37,38]. If the dye molecules are within 0-5nm of the metal surface, their fluorescence can get quenched, due to non-radiative energy transfer from the fluorophore to the metal, which is dissipated as heat[36]. For separations larger than 5nm, the fluorescence has been shown to increase, either due to an enhancement of the incident light field, especially around the edges of the nanoparticles, or due to an increase in the radiative decay rate[37, 38], i.e., the fluorescence quantum efficiency.

We have previously demonstrated the enhancement of two-photon fluorescence from a pH sensitive dye, 8-Hydroxypyrene-1,3,6-trisulfonic acid (HPTS), encapsulated inside a polyacrylamide nanoparticle containing a single silver nanosphere core[24]. The fluorescence intensity was enhanced up to 20 times, which was attributed to a combination of resonance energy transfer and the second harmonic generation by the silver core[24]. Recently, gold nanosphere clusters with a silica coating were shown to enhance the single photon fluorescence of porphyrine molecules[14]. Previously core shell nanoparticles with a single metal nanoparticle core have been used to enhance the single-photon fluorescence signal of Rhodamine 800 dye[39],as well as the second harmonic signals[40].However, here we do not observe any fluorescence enhancement from Rh-6G when incorporated inside the matrix. In fact, we observe a slight reduction in the fluorescence signal. This quenching can be attributed to the adsorption of the dye onto the metal surface (which on the other hand helps retain the dye inside the polymer matrix). Nonetheless, this nanoparticle design can enable simultaneous multimodal imaging contrast enhancement, such as fluorescence, photoacoustics (see below) and CT[14]. Additionally, the polymer matrix prevents the dye from interacting with plasma proteins, enzymes or macromolecules, thereby preserving its optical properties *in vivo*[22].

Specific targeting is achieved by modifying the surface of the polymer matrix and attaching the F3 peptide. The F3 peptide is a 31-amino acid fragment of the human high-mobility group-2 protein, and is used for specifically targeting tumor and tumor endothelial cells, which over-express the nucleolin receptor[41]. This ability to specifically target the 9L glioma cells, both *in vivo* and *in vitro*, has been previously investigated[25, 42, 43, 23]. The ability of the F3 peptide to selectively deliver the PAA nanoparticles to the nucleolin over-expressing tumor and tumor endothelial cells is shown in Figure S4. We observe a difference of about 300% between the accumulations of F3 targeted PAA NP and the non-targeted NP in the nucleolin overexpressing 9L cells. To ascertain that this is due to the over-expression of the nucleolin on the cell surface, we compare the results with the MCF7 cell line, which does not have significant over-expression of nucleolin on the cell surface. We observe significantly lower uptake for both the targeted and non targeted NP's in the MCF7 cells. Additionally, no difference between the uptake levels for the two types of NP is observed.

Photoacoustic Imaging

These nanoparticles can also act as good contrast agents for photoacoustic imaging, due to the high optical absorption coefficient of the metal clusters, and their practically zero

fluorescence quantum yield. The feasibility of these NP's for photoacoustic imaging was demonstrated by monitoring the optical contrast from blood vessels, with and without the nanoparticles. The nanoparticles were PEGylated for prolonging the circulation time in the blood stream. Previously it has been shown that the PEGylated polyacrylamide-based nanoparticles have a long plasma circulation time, of days ($t_{1/2}$=43 hours). A detailed study of the pharmacokinetics and bio-distribution of the PAA NP's has been presented previously[44].

Figure 7 shows photoacoustic microscopic images of the vasculature in a rat ear, before and after injecting the contrast agent. The NP's were injected into the caudal vein of the rat. We observe a 93% enhancement of contrast, at 10 minutes following NP injection. This looks quite promising, since blood by itself has a significantly high photoacoustic signal when irradiated at 532nm. Thus these nanoparticles have the potential to significantly improve the photoacoustic contrast, from any type of background tissue. For the present *in vivo* studies we used non-targeted NP's.

However the F3-targted NP's presented in the previous section, can specifically target nucleolin, which is overexpressed on the surfaces of certain tumor endothelial cells and thus can act as efficient markers for angiogenesis, as well as demarcate the tumor boundaries. Our previous *in vivo* experiments with F3 targeted PAA NPs, containing Coomassie Blue dye and iron oxide, have been used for delineating brain tumors visually[45], using photoacoustics[25] and MRI[42] respectively.

CONCLUSION

We presented the application and some practical advantages of using nanoclusters of silver nanoplates that are encapsulated in a polymeric matrix. The polymer matrix was utilised to increase the optical stability of the clusters, which would enhance their application as multimodal imaging contrast agents. Significant improvements were found for both fluorescence and photoacoustic imaging. The encapsulating matrix also reduced the cytotoxicity of the silver. Only at high concentrations were substantial ROS levels produced. While the main mechanism of cell death was found to be apoptosis, as the concentration and time of nanocluster incubation increased, so did the percentage of necrotic cells. These polymer encapsulated NC's have been modified for specific targeting, towards the 9L rat glioma cell line, by conjugating the F3 targeting peptide to the NP surface. The polymer-embedded nano-clusters also have the potential for use in X-Ray/CT Imaging applications, as a tool for early disease diagnostics, as well as for therapeutic applications, such as photothermal and photodynamic therapy.

Supplementary Material

Refer to Web version on PubMed Central for supplementary material.

Acknowledgments

This work was supported by NIH grant R01AR060350 (XW) and R01CA186769 (RK). The authors also acknowledge Mr.Teppei Shirakura for his help with the ICP measurement, Dr. Chao Tian for his help with

photoacoustic imaging, and Dr. Taeyuana Curry for her help with TEM imaging. The authors also thank the Chemistry department instrument facility and the Microscopy Imaging lab (MIL) at the University of Michigan.

References

(1). Fan JA, Wu C, Bao K, Bao J, Bardhan R, Halas NJ, Manoharan VN, Nordlander P, Shvets G, Capasso F. Self-Assembled Plasmonic Nanoparticle Clusters. Science. 2010; 328:1135–1138. [PubMed: 20508125]

(2). Romo-Herrera JM, Alvarez-Puebla RA, Liz-Marzán LM. Controlled Assembly of Plasmonic Colloidal Nanoparticle Clusters. Nanoscale. 2011; 3:1304–1315. [PubMed: 21229160]

(3). Lu Z, Yin Y. Colloidal Nanoparticle Clusters: Functional Materials by Design. Chemical Society Reviews. 2012; 41:6874. [PubMed: 22868949]

(4). Barnes WL, Dereux A, Ebbesen TW. Surface Plasmon Subwavelength Optics. Nature. 2003; 424:824–830. [PubMed: 12917696]

(5). Nie S. Probing Single Molecules and Single Nanoparticles by Surface-Enhanced Raman Scattering. Science. 1997; 275:1102–1106. [PubMed: 9027306]

(6). Taladriz-blanco P, Buurma NJ, Rodr L, Jorge P, Liz-marz LM, Herv P. Reversible Assembly of Metal Nanoparticles Induced by Penicillamine. Dynamic Formation of SERS Hot Spots. Journal of Material Chemistry. 2011; 21:16880–16887.

(7). Wenseleers W, Stellacci F, Meyer-Friedrichsen T, Mangel T, Bauer C. a, Pond SJK, Marder SR, Perry JW. Five Orders-of-Magnitude Enhancement of Two-Photon Absorption for Dyes on Silver Nanoparticle Fractal Clusters. The Journal of Physical Chemistry B. 2002; 106:6853–6863.

(8). Gill R, Le Ru EC. Fluorescence Enhancement at Hot-Spots: The Case of Ag Nanoparticle Aggregates. Phys. Chem. Chem. Phys. 2011; 13:16366–16372. [PubMed: 21837313]

(9). Yoon SJ, Mallidi S, Tam JM, Tam JO, Murthy A, Johnston KP, Sokolov KV, Emelianov SY. Utility of Biodegradable Plasmonic Nanoclusters in Photoacoustic Imaging. Opt. Lett. 2010; 35:3751–3753. [PubMed: 21081985]

(10). Guan Z, Gao N, Jiang X-F, Yuan P, Han F, Xu Q-H. Huge Enhancement in Two-Photon Photoluminescence of Au Nanoparticle Clusters Revealed by Single-Particle Spectroscopy. J. Am. Chem. Soc. 2013; 135:7272–7277. [PubMed: 23607514]

(11). Nabika H, Takase M, Nagasawa F, Murakoshi K. Toward Plasmon-Induced Photoexcitation of Molecules. J. Phys. Chem. Lett. 2010; 1:2470–2487.

(12). Wang S, Querner C, Dadosh T, Crouch CH, Novikov DS, Drndic M. Collective Fluorescence Enhancement in Nanoparticle Clusters. Nat. Commun. 2011; 2:364. [PubMed: 21694712]

(13). Urban AS, Shen X, Wang Y, Large N, Wang H, Knight MW, Nordlander P, Chen H, Halas NJ. Three-Dimensional Plasmonic Nanoclusters. Nano Lett. 2013; 13:4399–4403. [PubMed: 23977943]

(14). Hayashi K, Nakamura M, Miki H, Ozaki S, Abe M, Matsumoto T, Ishimura K. Gold Nanoparticle Cluster-Plasmon-Enhanced Fluorescent Silica Core-Shell Nanoparticles for X-Ray Computed Tomography-Fluorescence Dual-Mode Imaging of Tumors. Chem. Commun. (Camb). 2013; 49:5334–5336. [PubMed: 23648868]

(15). Pastoriza-Santos I, Liz-Marzán LM. Colloidal Silver Nanoplates. State of the Art and Future Challenges. Journal of Materials Chemistry. 2008; 18:1724.

(16). Homan, K. a; Souza, M.; Truby, R.; Luke, GP.; Green, C.; Vreeland, E.; Emelianov, S. Silver Nanoplate Contrast Agents for in Vivo Molecular Photoacoustic Imaging. ACS Nano. 2012; 6:641–650. [PubMed: 22188516]

(17). Charles DE, Aherne D, Gara M, Ledwith DM, Gun'ko YK, Kelly JM, Blau WJ, Brennan-Fournet ME. Versatile Solution Phase Triangular Silver Nanoplates for Highly Sensitive Plasmon Resonance Sensing. ACS Nano. 2010; 4:55–64. [PubMed: 20030362]

(18). Yang Y, Matsubara S, Xiong L, Hayakawa T, Nogami M. Solvothermal Synthesis of Multiple Shapes of Silver Nanoparticles and Their SERS Properties. J. Phys. Chem. C. 2007; 111:9095–9104.

(19). Aslan K, Lakowicz JR, Geddes CD. Rapid Deposition of Triangular Silver Nanoplates on Planar Surfaces: Application to Metal-Enhanced Fluorescence. J. Phys. Chem. B. 2005; 109:6247–6251. [PubMed: 16851692]

(20). Brandon MP, Ledwith DM, Kelly JM. Preparation of Saline-Stable, Silica-Coated Triangular Silver Nanoplates of Use for Optical Sensing. J. Colloid Interface Sci. 2014; 415:77–84. [PubMed: 24267332]

(21). Luke GP, Bashyam A, Homan K. a, Makhija S, Chen Y-S, Emelianov SY. Silica-Coated Gold Nanoplates as Stable Photoacoustic Contrast Agents for Sentinel Lymph Node Imaging. Nanotechnology. 2013; 24:455101. [PubMed: 24121616]

(22). Ray A, Kopelman R. Hydrogel Nanosensors for Biophotonic Imaging of Chemical Analytes. Nanomedine. 2013; 8:1829–1838.

(23). Ray A, Koo Lee Y-E, Epstein T, Kim G, Kopelman R. Two-Photon Nano-PEBBLE Sensors: Subcellular pH Measurements. Analyst. 2011; 136:3616–3622. [PubMed: 21773602]

(24). Ray A, Lee Y-EK, Kim G, Kopelman R. Two-Photon Fluorescence Imaging Super-Enhanced by Multishell Nanophotonic Particles, with Application to Subcellular pH. Small. 2012; 8:2213–2221. [PubMed: 22517569]

(25). Ray A, Wang X, Lee YK, Hah HJ, Kim G, Chen T, Orringer DA, Sagher O, Liu X, Kopelman R. Targeted Blue Nanoparticles as Photoacoustic Contrast Agent for Brain Tumor Delineation. Nano Research. 2011; 4:1163–1173.

(26). Xie Z, Chen S-L, Ling T, Guo LJ, Carson PL, Wang X. Pure Optical Photoacoustic Microscopy. Opt. Express. 2011; 19:9027–9034. [PubMed: 21643156]

(27). Xie Z, Roberts W, Carson P, Liu X, Tao C, Wang X. Evaluation of Bladder Microvasculature with High-Resolution Photoacoustic Imaging. Optics Letters. 2011; 36:4815. [PubMed: 22179893]

(28). Li F, Chen H, Zhang Y, Chen Z, Zhang Z-P, Zhang X-E, Wang Q. Three-Dimensional Gold Nanoparticle Clusters with Tunable Cores Templated by a Viral Protein Scaffold. Small. 2012; 8:3832–3838. [PubMed: 22911966]

(29). Haase A, Tentschert J, Jungnickel H, Graf P, Mantion A, Draude F, Plendl J, Goetz ME, Galla S, Mašić A, Thuenemann AF, Taubert A, Arlinghaus HF, Luch A. Toxicity of Silver Nanoparticles in Human Macrophages: Uptake, Intracellular Distribution and Cellular Responses. Journal of Physics: Conference Series. 2011; 304:012030.

(30). AshaRani PV, Low Kah Mun G, Hande MP, Valiyaveettil S. Cytotoxicity and Genotoxicity of Silver Nanoparticles in Human Cells. ACS Nano. 2009; 3:279–290. [PubMed: 19236062]

(31). Pal S, Tak YK, Song JM. Does the Antibacterial Activity of Silver Nanoparticles Depend on the Shape of the Nanoparticle? A Study of the Gram-Negative Bacterium Escherichia Coli. Appl. Environ. Microbiol. 2007; 73:1712–1720. [PubMed: 17261510]

(32). Foldbjerg R, Olesen P, Hougaard M, Dang DA, Hoffmann HJ, Autrup H. PVP-Coated Silver Nanoparticles and Silver Ions Induce Reactive Oxygen Species, Apoptosis and Necrosis in THP-1 Monocytes. Toxicol. Lett. 2009; 190:156–162. [PubMed: 19607894]

(33). Kim S, Choi JE, Choi J, Chung K-H, Park K, Yi J, Ryu D-Y. Oxidative Stress-Dependent Toxicity of Silver Nanoparticles in Human Hepatoma Cells. Toxicol. In Vitro. 2009; 23:1076–1084. [PubMed: 19508889]

(34). George S, Lin S, Ji Z, Thomas CR, Li L, Mecklenburg M, Meng H, Wang X, Zhang H, Xia T, Hohman JN, Lin S, Zink JI, Al GET. Surface Defects on Plate-Shaped Silver Nanoparticles Contribute to Its Hazard Potential in a Fish Gill Cell Line and Zebra Fi Sh Embryos. 2012:3745–3759.

(35). Elliott MR, Ravichandran KS. Clearance of Apoptotic Cells: Implications in Health and Disease. 2010; 189:1059–1070.

(36). Anger P, Bharadwaj P, Novotny L. Enhancement and Quenching of Single-Molecule Fluorescence. Phys. Rev. Lett. 2006; 96:113002. [PubMed: 16605818]

(37). Aslan K, Gryczynski I, Malicka J, Matveeva E, Lakowicz JR, Geddes CD. Metal-Enhanced Fluorescence: An Emerging Tool in Biotechnology. Curr. Opin. Biotechnol. 2005; 16:55–62. [PubMed: 15722016]

(38). Lin C-Y, Chiu K-C, Chang C-Y, Chang S-H, Guo T-F, Chen S-J. Surface Plasmon-Enhanced and Quenched Two-Photon Excited Fluorescence. Opt. Express. 2010; 18:12807–12817. [PubMed: 20588409]

(39). Aslan K, Wu M, Lakowicz JR, Geddes CD. Fluorescent Core-Shell Ag@SiO2 Nanocomposites for Metal-Enhanced Fluorescence and Single Nanoparticle Sensing Platforms. J. Am. Chem. Soc. 2007; 129:1524–1525. [PubMed: 17283994]

(40). Clark HA, Campagnola PJ, Wuskell JP, Lewis A, Loew LM, June RV. Second Harmonic Generation Properties of Fluorescent Polymer-Encapsulated Gold Nanoparticles. 2000:10234–10235.

(41). Porkka K, Laakkonen P, Hoffman JA, Bernasconi M, Ruoslahti E. A Fragment of the HMGN2 Protein Homes to the Nuclei of Tumor Cells and Tumor Endothelial Cells in Vivo. Proc. Natl. Acad. Sci. U. S. A. 2002; 99:7444–7449. [PubMed: 12032302]

(42). Reddy GR, Bhojani MS, McConville P, Moody J, Moffat BA, Hall DE, Kim G, Koo Y-EL, Woolliscroft MJ, Sugai JV, Johnson TD, Philbert MA, Kopelman R, Rehemtulla A, Ross BD. Vascular Targeted Nanoparticles for Imaging and Treatment of Brain Tumors. Clin. Cancer Res. 2006; 12:6677–6686. [PubMed: 17121886]

(43). Orringer DA, Koo Y-EL, Chen T, Kim G, Hah HJ, Xu H, Wang S, Keep R, Philbert MA, Kopelman R, Sagher O. In Vitro Characterization of a Targeted, Dye-Loaded Nanodevice for Intraoperative Tumor Delineation. Neurosurgery. 2009; 64:965–971. [PubMed: 19404156]

(44). Wenger Y, Schneider RJ, Reddy GR, Kopelman R, Jolliet O, Philbert MA. Tissue Distribution and Pharmacokinetics of Stable Polyacrylamide Nanoparticles Following Intravenous Injection in the Rat. Toxicol. Appl. Pharmacol. 2011; 251:181–190.

(45). Nie G, Hah HJ, Kim G, Lee YE, Qin M, Ratani TS, Fotiadis P, Miller A, Kochi A, Gao D, Chen T, Orringer DA, Sagher O, Philbert MA, Kopelman R. Hydrogel nanoparticles with covalently linked coomassie blue for brain tumor delineation visible to the surgeon. Small. 2012; 8(6):884–91. [PubMed: 22232034]

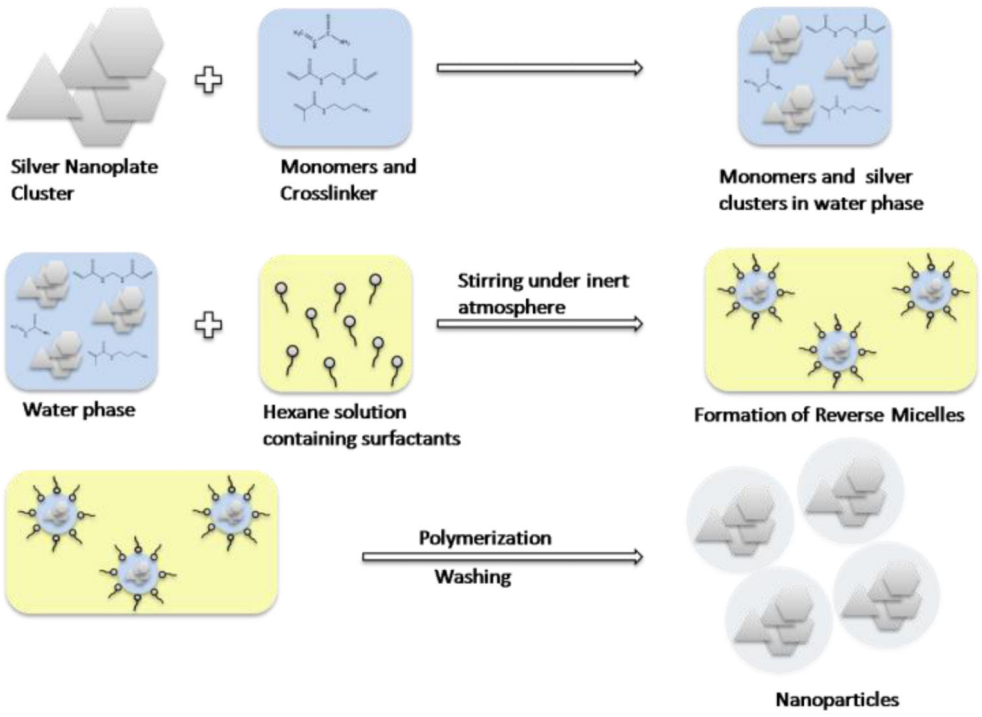

Fig 1.
Schematic of composite nanoparticle synthesis

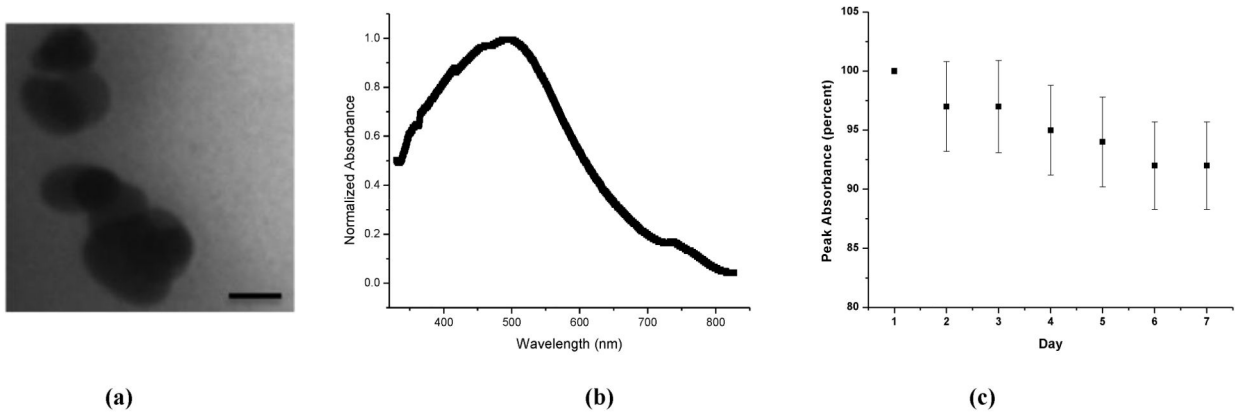

Fig 2.

(a) TEM image of the composite nanoparticles. (Scale 25 nm) (b) Absorbance spectra of the nanoparticles. (c) Changes in absorption (at 500nm), monitored over 7 days.

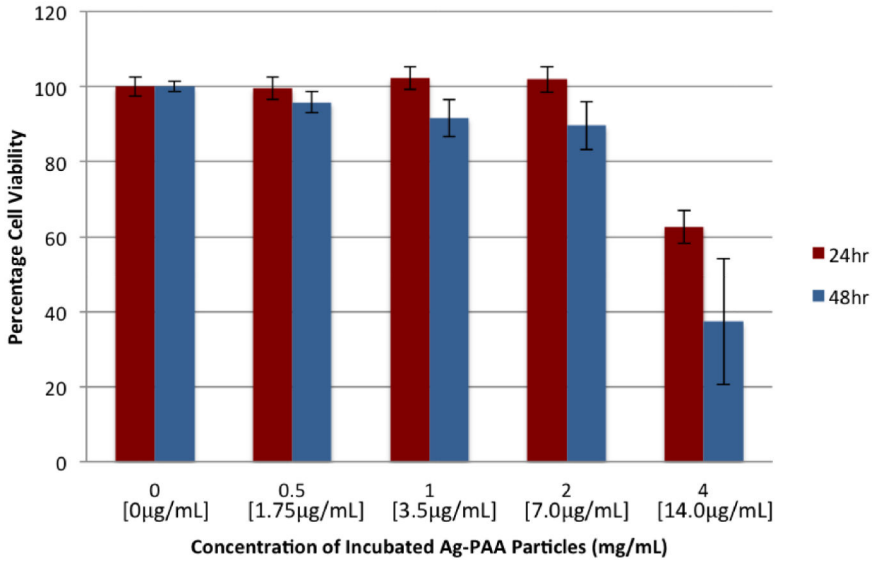

Fig 3.

9L cell Cytotoxicity of the polymer coated silver nanoparticles. The silver concentration is shown in brackets.

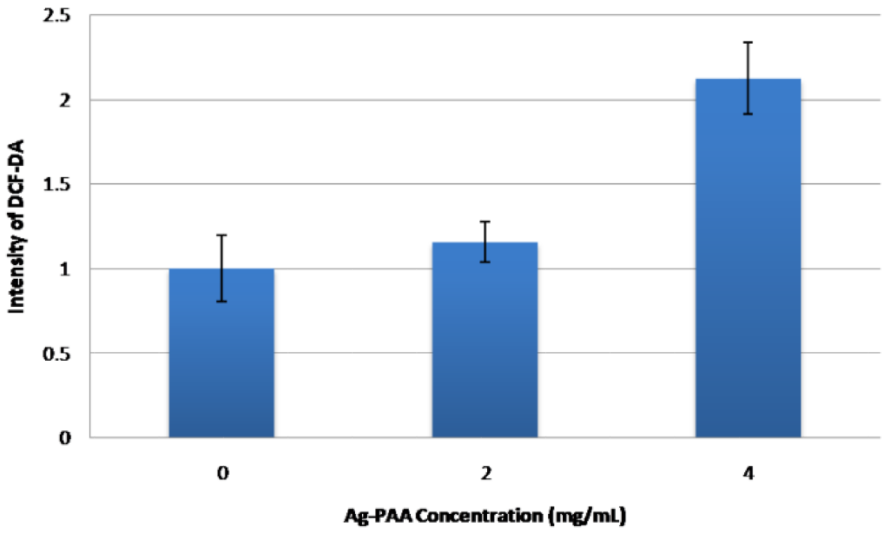

Fig 4.
Oxidative stress in 9L cells *vs.* concentration of NP's.

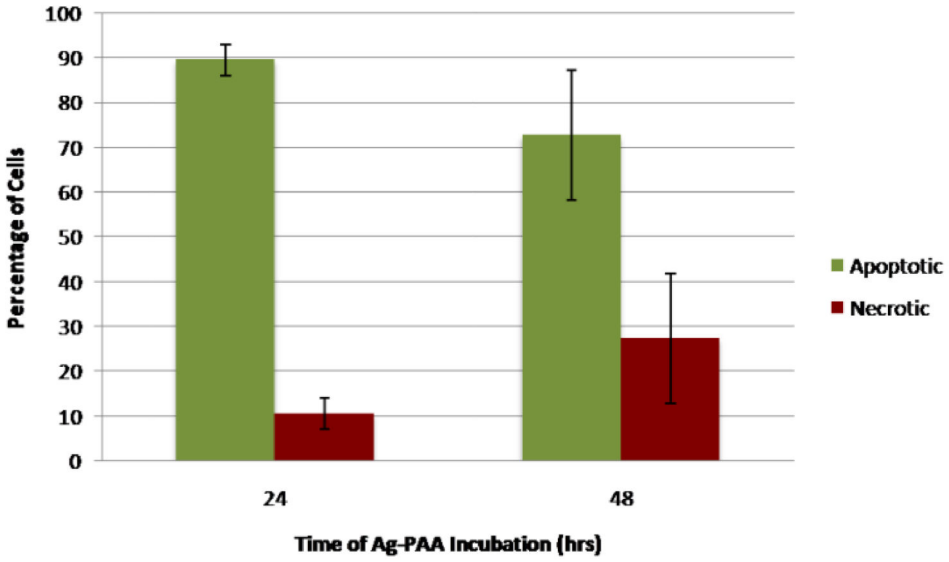

Fig 5.
Cell death mechanism with incubation by silver nanoplates after 24 and 48 hours.

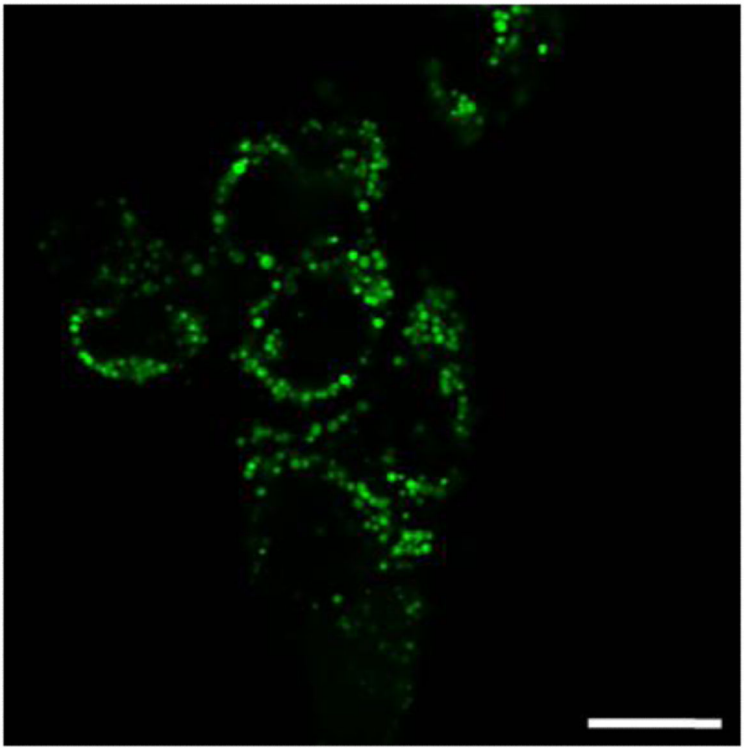

Fig 6.
Fluorescence image of the 9L rat glioma cells containing the Rh-6G embedded nanoparticles (Scale 20μm).

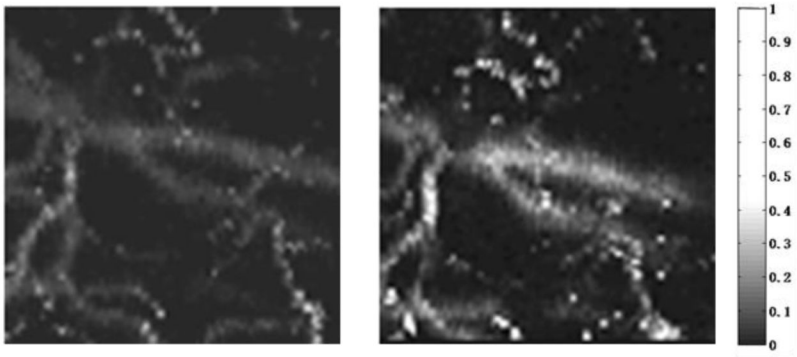

Fig 7.

Photoacoustic image (700μm×700μm) of the vasculature in a rat ear, before (left) and after (right) the injection of the nanoparticle contrast agent.